Metabolic Engineering 81 (2024) 88–99

Contents lists available at ScienceDirect

Metabolic Engineering

journal homepage: www.elsevier.com/locate/meteng

Comparison of wild-type KT2440 and genome-reduced EM42 *Pseudomonas putida* strains for muconate production from aromatic compounds and glucose

Caroline R. Amendola [a,b], William T. Cordell [a,c], Colin M. Kneucker [a,b], Caralyn J. Szostkiewicz [a,b], Morgan A. Ingraham [a,b], Michela Monninger [a,b], Rosemarie Wilton [b,d], Brian F. Pfleger [c], Davinia Salvachúa [a,b], Christopher W. Johnson [a,b,**], Gregg T. Beckham [a,b,*]

[a] Renewable Resources and Enabling Sciences Center, National Renewable Energy Laboratory, Golden, CO, 80401, USA
[b] Agile BioFoundry, Emeryville, CA, 94608, USA
[c] Department of Chemical and Biological Engineering, University of Wisconsin-Madison, Madison, WI, USA
[d] Biosciences Division Argonne National Laboratory, Lemont, IL, 60439, USA

ARTICLE INFO

Keywords:
Pseudomonas putida KT2440
Pseudomonas putida EM42
genome reduction
Muconic acid
Aromatic catabolism

ABSTRACT

Pseudomonas putida KT2440 is a robust, aromatic catabolic bacterium that has been widely engineered to convert bio-based and waste-based feedstocks to target products. Towards industrial domestication of *P. putida* KT2440, rational genome reduction has been previously conducted, resulting in *P. putida* strain EM42, which exhibited characteristics that could be advantageous for production strains. Here, we compared *P. putida* KT2440- and EM42-derived strains for *cis,cis*-muconic acid production from an aromatic compound, *p*-coumarate, and in separate strains, from glucose. To our surprise, the EM42-derived strains did not outperform the KT2440-derived strains in muconate production from either substrate. In bioreactor cultivations, KT2440- and EM42-derived strains produced muconate from *p*-coumarate at titers of 45 g/L and 37 g/L, respectively, and from glucose at 20 g/L and 13 g/L, respectively. To provide additional insights about the differences in the parent strains, we analyzed growth profiles of KT2440 and EM42 on aromatic compounds as the sole carbon and energy sources. In general, the EM42 strain exhibited reduced growth rates but shorter growth lags than KT2440. We also observed that EM42-derived strains resulted in higher growth rates on glucose compared to KT2440-derived strains, but only at the lowest glucose concentrations tested. Transcriptomics revealed that genome reduction in EM42 had global effects on transcript levels and showed that the EM42-derived strains that produce muconate from glucose exhibit reduced modulation of gene expression in response to changes in glucose concentrations. Overall, our results highlight that additional studies are warranted to understand the effects of genome reduction on microbial metabolism and physiology, especially when intended for use in production strains.

1. Introduction

Genome reduction is an appealing strategy for improving biocatalysts (Ara et al., 2007; Giga-Hama et al., 2007; Mizoguchi et al., 2007; Juhas et al., 2014; Kurokawa and Ying, 2020; Calvey et al., 2023), and this approach has been successfully used in several microbial hosts to improve growth, production, tolerance to a variety of compounds, genetic tractability, and other beneficial phenotypes (Pósfai et al., 2013; Lee et al., 2009; Suárez et al., 2019; Yan et al., 2018; Zhang et al., 2020). Although genome-reduction has the potential to improve biocatalysts, this strategy does not universally lead to beneficial phenotypes, and it yields mixed results depending on the context and host (Mizoguchi et al., 2007; Lee et al., 2009; Kurokawa and Ying, 2020; Choe et al., 2016; Hashimoto et al., 2005; Kolisnychenko et al., 2002; Komatsu et al., 2010; Park et al., 2014; Pósfai et al., 2013; Yu et al., 2002; Hemmerich et al., 2020; Calvey et al., 2023). To date, several bacteria from the genus

* Corresponding author. Renewable Resources and Enabling Sciences Center, National Renewable Energy Laboratory, Golden, CO, 80401, USA.
** Corresponding author. Renewable Resources and Enabling Sciences Center, National Renewable Energy Laboratory, Golden, CO, 80401, USA.
E-mail addresses: christopher.johnson@nrel.gov (C.W. Johnson), gregg.beckham@nrel.gov (G.T. Beckham).

https://doi.org/10.1016/j.ymben.2023.11.004
Received 2 August 2023; Received in revised form 12 November 2023; Accepted 19 November 2023
Available online 23 November 2023

Pseudomonas have been subjected to genome reduction (Fan et al., 2020; Martínez-García et al., 2014a; Wynands et al., 2019). For example, 7.7% genome-reduced *Pseudomonas mendocina* showed enhanced production of polyhydroxyalkanoates and alginate oligosaccharide (Fan et al., 2020) and 10% genome-reduced *Pseudomonas taiwanensis* exhibited improved solvent tolerance, growth rate, biomass yields, and phenol production (Wynands et al., 2019) compared to the parent strain. These results highlight some positive effects achieved using genome reduction in *Pseudomonas* species.

Of note among the Pseudomonads, *Pseudomonas putida* KT2440 (hereafter KT2440) has also been subjected to genome reduction (Martínez-García et al., 2014a; Liang et al., 2020). KT2440 is a Gram-negative soil bacterium that has promise as a production host to convert bio-based and waste-based feedstocks to value-added compounds (Nikel and de Lorenzo, 2018; Nikel et al., 2014; Weimer et al., 2020). KT2440 has many traits that make it an ideal candidate as a biocatalyst, such as high stress tolerance, diverse metabolic pathways, and genetic tractability (Martin-Pascual et al., 2021; Nikel et al., 2016; Nikel and de Lorenzo 2014). KT2440 can consume multiple aromatic compounds as carbon sources through well-characterized aromatic catabolic pathways (Jiménez et al., 2002). This capability has been leveraged to engineer strains able to produce molecules such as *cis*, *cis*-muconate from lignin-derived aromatic compounds (Vardon et al., 2015) (Fig. 1A). *P. putida* is also able to utilize glucose via a combination of the Entner-Doudoroff, gluconeogenic Embden-Meyerhof-Parnas, and pentose phosphate pathways termed the EDEMP cycle (Nikel et al., 2015), which has been exploited to engineer strains capable of producing muconate from glucose (Bentley et al., 2020; Draths and Frost 1994; Johnson et al., 2016, 2019; Ling et al., 2022) (Fig. 1B). Muconate is a 'bioprivileged' molecule that can be converted to both direct replacement chemicals and performance-advantaged bioproducts (Almqvist et al., 2021; Cywar et al., 2022; Johnson et al., 2019; Kohlstedt et al., 2018; Linger et al., 2014; Rorrer et al., 2019; Salvachúa et al., 2018; Shanks and Keeling 2017; Sonoki et al., 2014; van Duuren et al., 2020; Vardon et al., 2016).

EM42, a genome-reduced strain derived from KT2440, was constructed using an I-SceI endonuclease-enabled methodology to make genomic deletions (Martínez-García and de Lorenzo, 2011). Ten genomic deletions were made in EM42 that reduced the genome by 4% (Martínez-García et al., 2014a). EM42 and its derivatives have been shown to have numerous benefits compared to KT2440, including a reduced growth lag phase, improved biomass yield, increased intracellular ATP, as well as increased intracellular NADPH/NADP+ ratios (Martínez-García et al., 2014a; Martínez-García et al., 2014b). Increased genomic stability, increased tolerance to stressors, increased heat tolerance, and improved heterologous protein expression have also been

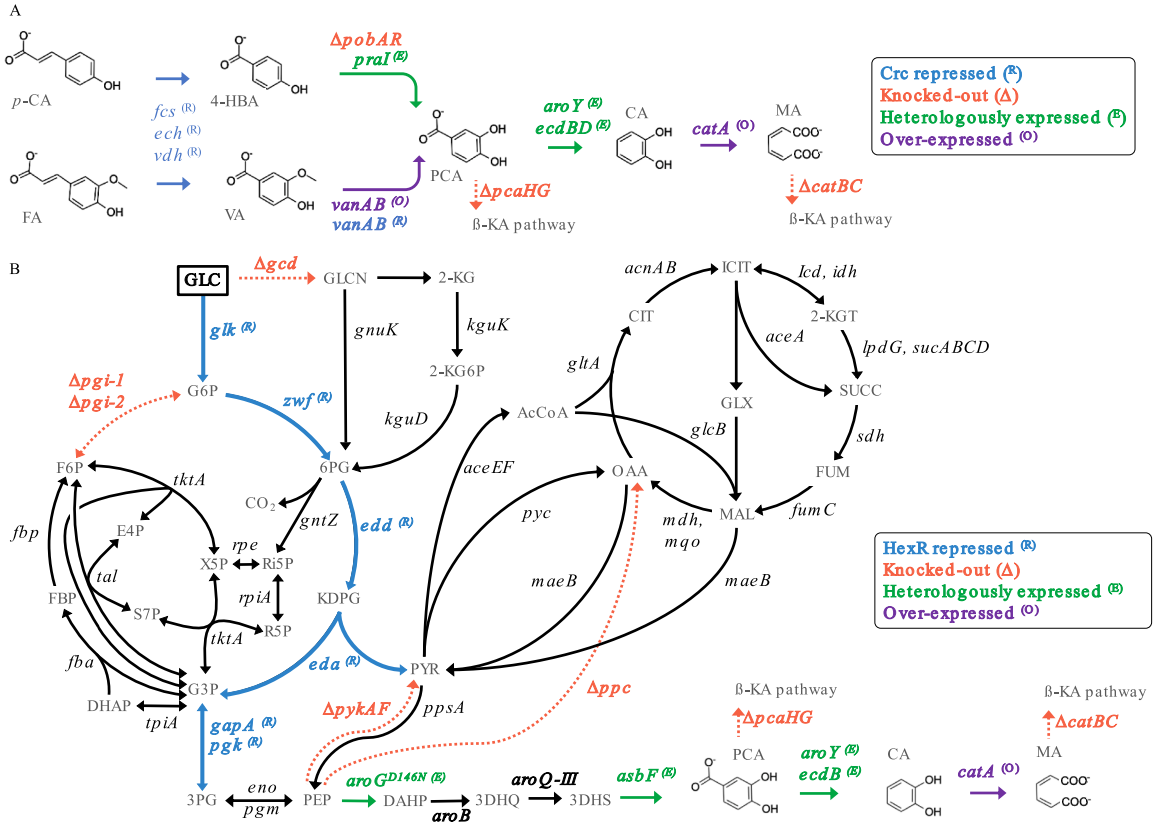

Fig. 1. Metabolic pathways for *cis*,*cis*-muconate production in engineered *P. putida* strains.
(**A**) Pathway to produce muconate from aromatic compounds. Genes believed to be repressed by Crc are shown in blue, deletions are shown in orange, heterologously expressed genes are in green, and native *P. putida* genes that have been over-expressed are in purple. Abbreviations: *p*-CA; *p*-coumarate, FA; ferulate, 4HBA; 4-hydroxybenzoate, VA; vanillate, PCA; protocatechuate, CA; catechol, MA; muconate. (**B**) Pathway for the production of muconate from glucose, modified from Bentley et al., (2020). Gene deletions are highlighted in red, heterologously expressed genes are highlighted in green, native *P. putida* genes that have been overexpressed are in purple, and genes regulated by HexR are shown in blue. Abbreviations: P; phosphate, GLC; glucose, GLCN; gluconate, 2-KG; 2-ketogluconate, 2-KG6P; 2-ketogluconate-6-P, G6P; glucose-6-P, 6 PG; 6-phosphogluconate, KDPG; 2-keto-3- deoxy-6-phosphogluconate, G3P; glyceraldehyde-3-P, FBP; fructose-1,6-P2, F6P; fructose-6-P, X5P; xylose-5-P, S7P; sedoheptulose-7-P, E4P; erythrose-4-P, R5P; ribose-5-P, Ri5P; ribulose-5-P, 3 PG; glycerate-3-P, PEP; phosphoenolpyruvate, DHAP; dihydroxyacetone-P, DAHP; 3-deoxy-D-arabinoheptulosonate 7-phosphate, 3DHQ; 3-dehydroxyquinate, ICIT; isocitrate, CIT; citrate, AKG; alpha-ketoglutarate, SUCC; succinate, FUM; fumarate, MAL; malate, GLX; glyoxylate, OAA; oxaloacetate, AcCoA; acetyl-Coenzyme A, PYR; pyruvate, PCA; protocatechuic acid, CA; catechol, MA; muconate.

demonstrated in genome-reduced *P. putida* strains (Aparicio et al., 2019; Lieder et al., 2015; Liang et al., 2020, 2021). EM42 has also been shown to be more tolerant to wastewater generated from catalytic fast pyrolysis of lignocellulosic biomass than KT2440 and evaluated for wastewater valorization (Jayakody et al., 2018; Henson et al., 2021). In addition to EM42, other studies have also demonstrated that deletion of genomic islands is beneficial in KT2440 and increased the ability of the bacterium to convert lignin-derived compounds to polyhydroxyalkanoates (Liang et al., 2020; Kohlstedt et al., 2022; Zong et al., 2022). Together, these results highlight the utility of genome reduction in KT2440.

There are few direct comparisons between EM42- and KT2440-derived strains engineered to produce a single target compound. Recent work from Kohlstedt et al., compared EM42- and KT2440-derived strains to produce muconate from catechol (Kohlstedt et al., 2022). Kohlstedt et al. found that the EM42-derived production strain was more tolerant to catechol, which resulted in reduced lag, faster muconate production in shake flask cultivations, and higher titers of muconate from catechol (up to 74 g/L) in bioreactors compared to the equivalent KT2440-derived strain (up to 62 g/L) (Kohlstedt et al., 2022).

In this work, we sought to directly compare KT2440- and EM42-derived strains engineered to produce muconate from two lignocellulosic-derived carbon sources, *p*-coumarate and glucose, using previously engineered strains (Bentley et al., 2020; Kuatsjah et al., 2022) and constructed equivalent EM42-derived strains. We observed that the EM42-derived strains did not outperform the KT2440-derived strains in muconate production from either *p*-coumarate or glucose in either flask or bioreactor cultivations. To better understand the performance of the parent strains, we analyzed growth profiles of KT2440 and EM42 on aromatic compounds as the sole carbon and energy sources. We observed that EM42 exhibited shorter growth lags, but reduced growth rates compared to KT2440. Additionally, we observed that EM42-derived strains resulted in higher growth rates on glucose compared to KT2440-derived strains, but only at the lowest glucose concentrations tested; when the concentration of glucose was increased, performance was diminished. Transcriptomics revealed that genome reduction in EM42 had global effects on transcript levels relative to KT2440, specifically in terms of reduced modulation of gene expression in response to changes in glucose concentrations.

2. Materials and methods

2.1. Plasmid construction

Construction details for previously published plasmids can be found in Bentley et al. (2020); Kuatsjah et al. (2022). A list of all plasmids used for strain construction can be found in Table S1. The plasmids pCA006 and pCA029 were cloned by TWIST Biosciences (Table S2).

2.2. Strain construction

Competent *P. putida* cells were made by following a previously published protocol (Choi et al., 2006). A volume of 50 μL of competent *P. putida* cells were mixed with 300–500 ng of plasmid and electroporated (Choi et al., 2006). Cells were recovered for 1 h at 30 °C with shaking at 225 rpm in 950 μL of SOC media (0.2 g/L tryptone, 0.05 g/L yeast extract, 10 mM NaCl, 2.5 mM KCl, 10 mM $MgCl_2$, 10 mM $MgSO_4$, and 20 mM glucose). After recovery, cells were plated on lysogenic broth (LB) (Miller) agar plates containing 50 μg/mL kanamycin. Sucrose counterselection was performed by following a previously published method (Johnson and Beckham, 2015). Colony PCR with MyTaqTM HS Red Mix (Bioline) was used to confirm gene replacements and deletions.

2.3. Shake flask cultivations

Seed cultures for shake flask cultivations were inoculated from glycerol stocks into 5 mL of LB (Miller) medium in 14 mL culture tubes. Seed cultures were grown overnight at 30 °C and 225 rpm. From the overnight cultures, a second seed culture was inoculated into LB at a starting optical density at 600 nm (OD_{600}) of 0.2. The second seed culture was grown to an OD_{600} of 2.0. Once at the appropriate OD_{600}, the cultures were pelleted by centrifugation at 4500 rpm, and the pellets were washed with 1x M9 salts. Shake flasks were inoculated to an OD_{600} of 0.1. Shake flask cultivations were conducted in 25 mL of M9 minimal media (pH 7, 6.78 g/L Na_2HPO_4, 3 g/L KH_2PO_4, 0.5 g/L NaCl, 1 g/L NH4Cl, 2 mM $MgSO_4$, 100 μM $CaCl_2$, and 18 μM $FeSO_4$). For strains that produce muconate from aromatic compounds, the M9 minimal media was supplemented with 20 mM *p*-coumaric acid (*p*-CA) for conversion of muconate and 10 mM glucose for growth. Subsequently, 10 mM glucose was fed at 24 and 48 h. For strains that produce muconate from glucose, the M9 minimal media was supplemented with 30 mM glucose for growth and conversion to muconate. 1 mL Samples were taken periodically throughout the cultivations for bacterial growth (OD_{600}) measurements and for metabolite analysis.

2.4. Genome sequencing and assembly

Strains were cultured overnight at 30 °C in LB broth, and the genomic DNA was extracted with the Monarch HMW DNA Extraction Kit for Tissue (New England Biolabs) according to the manufacturer's instructions. For Nanopore sequencing, DNA libraries were prepared according to the protocol for ligation sequencing of gDNA with native barcoding using SQK-LSK109 with EXP-NBD104 (Oxford Nanopore Technologies). Libraries were sequenced on a MinION using an R9.4.1 flow cell. For Illumina sequencing, the DNA was fragmented with a Covaris Focused-ultrasonicator followed by automated library preparation with an Apollo 324 system using the PrepX DNA Library Kit (Takara Bio). Libraries were size selected with a BluePippin (Sage Science) and sequenced on a Nextseq 2000 using Illumina P1 reagents and generating 150 bp paired-end reads. Quality control, read filtering and base correction of the FASTQ data were performed with fastp v0.12.4 (Chen et al., 2018).

Nanopore data was base-called with Guppy v6.1.3 using the super accuracy basecalling model (SUP). Using Filtlong v0.2.1, the reads were filtered to a minimum length of 1000 bases, and the top 95% of these reads (based on read length) were carried forward. Trycycler v0.5.3 (Wick et al., 2021) was used to produce consensus assemblies from the Nanopore data. The input assemblies were generated with Flye v2.9.1-b1780 (Kolmogorov et al., 2019), Raven v1.8.1 (Vaser and Šikić, 2021), and Miniasm/Minipolish v0.3-r179/v0.1.3 (Wick and Holt, 2019). Long-read polishing of the consensus assemblies was then performed with Medaka v1.6.1 using the model r941_min_sup_g613. Finally, each long-read polished assembly was polished again with the Illumina short-read data using Polypolish v0.5.0 (Wick and Holt, 2022).

2.5. Plate reader cultivations

Overnight cultures were started by inoculating 5 mL LB (Miller) medium from glycerol stocks into 14 mL tubes. Cultures were incubated overnight at 30 °C and 225 rpm. M9 medium supplemented with the various carbon sources were prepared fresh for each cultivation. The cells were centrifuged at 4000 rpm for 5 min then resuspended in 1 mL 1x M9 salts and washed again. The pellet was resuspended in 1x M9 salts and the OD_{600} was measured. The cells were diluted to an OD of 0.1 in M9 minimal media supplemented with *p*-CA, FA, 4-HBA, VA, PCA, CA, BA or glucose. For each well, 200 μL of cells were aliquoted in triplicate into a microtiter plate. Non-inoculated solutions were included as controls. Growth was measured using a Bioscreen C Pro (Growth Curves USA). Growth rates were calculated using Growth Curve Fitting software Version 0.3. Maximum OD_{600} were calculated using GraphPad Prism.

2.6. Production of muconate from p-coumarate in bioreactors

Seed cultures were inoculated from glycerol stocks into 50 mL of LB (Miller) medium in 250 mL baffled flasks. These flasks were incubated for 16 h at 30 °C and 225 rpm. Then, the broths were centrifuged (8 min at 5000×*g*), the supernatant discarded, and the cells resuspended in modified M9 minimal medium for inoculation in the bioreactors (5 mL) at an initial OD_{600} of 0.2. Bioreactor cultivations were performed in 0.5 L bioreactors (BioStat-Q Plus, Sartorius Stedim Biotech) at an initial working volume of 250 mL. The batch medium consisted of modified M9 minimal media (pH 7, 13.55 g/L Na_2HPO_4, 6 g/L KH_2PO_4, 1 g/L NaCl, 2.25 g/L $(NH_4)_2SO_4$, 2 mM $MgSO_4$, 100 μM $CaCl_2$, and 18 μM $FeSO_4$) plus 2.7 g/L glucose as a carbon source. The feeding medium consisted of a solution of *p*-coumarate, glucose, 13.5 g/L $(NH_4)_2SO_4$, and 4 mL/L antifoam 204. The molar ratio of *p*-coumarate to glucose was tested at two ratios, 2:1 (109 g of *p*-coumarate and 66.5 g/L glucose) and 8:1 (123 g of *p*-coumarate or 14.85 g/L of glucose). The feeding medium was adjusted to pH 9.3 with 10 N NaOH. The bioreactors were controlled at 30 °C and at pH 7 by the addition of 4 N NH_4OH. Agitation speed was initiated at 350 rpm and was automatically modified to maintain a saturation of dissolved oxygen of 30% during the cultivation. After 4 h within the batch phase, 2 mM *p*-coumarate was added to the bioreactors to induce the cells. The fed-batch phase started when glucose was depleted in the batch phase (~8 h). The feeding rate was constant to add 5 mmol *p*-coumarate/L/h (value based on the initial volume of the reactor). Samples were taken periodically for bacterial growth (OD_{600}) measurements and for metabolite analysis.

2.7. Production of muconate from glucose in bioreactors

Seed cultures were inoculated from glycerol stocks into 50 mL of LB (Miller) medium in 250 mL baffled flasks. These flasks were incubated for 16 h at 30 °C and 225 rpm. Then, the cells were again inoculated in 50 mL LB (Miller) medium in 250 mL flasks at an initial OD_{600} of 0.2. After 4 h of incubation, the broths were centrifuged (8 min at 5000×*g*), the supernatant discarded, and the cells resuspended in modified M9 minimal medium for inoculation in the bioreactors (5 mL) at an initial OD_{600} of 0.2. Bioreactor cultivations were performed in 0.5 L bioreactors (BioStat-Q Plus, Sartorius Stedim Biotech) at an initial working volume of 250 mL. The batch medium consisted of M9 minimal media (pH 7, 13.55 g/L Na_2HPO_4, 6 g/L KH_2PO_4, 1 g/L NaCl, 2.25 g/L $(NH_4)_2SO_4$, 2 mM $MgSO_4$, 100 μM $CaCl_2$, and 36 μM $FeSO_4$) plus 25 g/L glucose as a carbon source. The fed-batch medium consisted of a solution of 500 g/L glucose and 4 mL/L antifoam 204. The bioreactors were controlled at 30 °C and at pH 7 by the addition of 4 N NH_4OH. Agitation speed was initiated at 350 rpm and was automatically modified to maintain a saturation of dissolved oxygen of 30% during the cultivation. The fed-batch phase started when glucose was lower than 10 g/L and the feeding rate was manually controlled to maintain glucose concentrations in the bioreactor between 1 and 10 g/L. Samples were taken periodically for bacterial growth (OD_{600}) measurements and for metabolite analysis.

2.8. Metabolite analysis

Muconate and aromatic compounds were analyzed as previously described (Bleem et al., 2022). *cis,cis*-Muconate and *cis,trans*-muconate standards were prepared as previously described (Pleitner et al., 2019). A minimum of 6 calibration levels for each analyte were utilized to create linear calibration curves with ranges of 1 μg/mL to 500 μg/mL and an r^2 coefficient greater than or equal to 0.995. A quantitative wavelength of 265 nm was used for all analytes. To monitor the system for stability, a calibration verification standard was injected every 15 samples. Analysis of glucose was analyzed by high performance liquid chromatography utilizing an Aminex HPX-87H column (Bio-Rad Laboratories) as described previously (Notonier et al., 2021).

2.9. Transcriptomics

Cultures for transcriptomics experiments were set up in the same manner as the shake flask cultivations. For the comparison between KT2440 and EM42, the media was supplemented with 50 mM *p*-coumarate. For the comparison between CA055 and GB062, the media was supplemented with either 10 mM or 30 mM glucose. After growing to mid-exponential phase, cells were harvested by centrifugation at 4500 rpm for 5 min. The cell pellets were flash frozen and sent to AZENTA Life Sciences for RNA library preparation and sequencing.

RNA samples were quantified using a Qubit 2.0 Fluorometer (ThermoFisher Scientific) and RNA integrity was checked with 4200 TapeStation (Agilent Technologies). The rRNA depletion sequencing libraries were prepared by using the QIAGEN FastSelect rRNA Bacteria Kit (Qiagen). RNA sequencing library preparation used NEBNext Ultra II RNA Library Preparation Kit for Illumina by following the manufacturer's recommendations (NEB). Enriched RNAs were fragmented for 15 min at 94 °C. First strand and second strand cDNA were subsequently synthesized. cDNA fragments were end repaired and adenylated at 3'ends, and universal adapters were ligated to cDNA fragments, followed by index addition and library enrichment with limited cycle PCR. Sequencing libraries were validated using the Agilent Tapestation 4200 (Agilent Technologies) and quantified using the Qubit 2.0 Fluorometer (ThermoFisher Scientific) as well as by quantitative PCR (KAPA Biosystems). The sequencing libraries were multiplexed and clustered on one lane of a flowcell. After clustering, the flowcell was loaded on the Illumina HiSeq instrument (4000 or equivalent) according to the manufacturer's instructions. The samples were sequenced using a 2 × 150 Paired End configuration. Image analysis and base calling were conducted by the HiSeq Control Software (HCS).

Raw sequence data (.bcl files) generated from Illumina HiSeq were converted into fastq files and de-multiplexed using the Illumina bcl2fastq program version 2.20. One mismatch was allowed for index sequence identification. Data analysis was performed by AZENTA Life Sciences. Briefly, the reads were trimmed and mapped to a reference genome using Bowtie2 aligner v.2.2.6. Gene hit counts were calculated and extracted to gene hit count tables and used for differential gene expression analysis. DESeq2 was used to compare gene expression between groups. The Wald test was used to generate p-values and log2 fold changes. Genes with an adjusted p-value of <0.05 and $\log_2$ fold-change $>|1|$ were considered differentially expressed. DeepVenn was used to generate Venn diagrams (Hulsen, 2022).

3. Results

3.1. EM42-derived strains do not exhibit improved muconate production from p-coumarate compared to KT2440-derived strains in shake flasks

We first engineered *P. putida* EM42 to produce muconate from hydroxycinnamic acids, such as *p*-coumarate (Fig. 1A), generating strain CJ921. Then, we compared the performance of CJ921 to the equivalent *P. putida* KT2440-derived strain, CJ781, using shake flask cultivations (Fig. 2, Table S3A) (Kuatsjah et al., 2022). Overall, CJ921 did not outperform CJ781 in terms of growth, intermediate buildup, or production of muconate. One of the beneficial phenotypes of EM42 is increased NADPH availability (Martínez-García et al., 2014a). Limited amounts of NADPH can be a detriment to production strains, and it was previously improved in CJ781 by replacing the native 4-HBA hydroxylase PobA, which uses only NADPH as a cofactor, and the transcription factor that drives its expression, PobR, with the heterologous enzyme PraI, which can utilize NADPH or NADH (Kuatsjah et al., 2022). To determine if EM42-derived strains would outperform KT2440-derived strains when NADPH was limited, we constructed strains expressing *pobAR*, where NADPH should be limiting, or both *pobAR* and *praI*, where it should not (Table 1). When CJ475 (expressing *pobAR*) was compared to the equivalent EM42-derived strain CJ916, we observed that CJ916

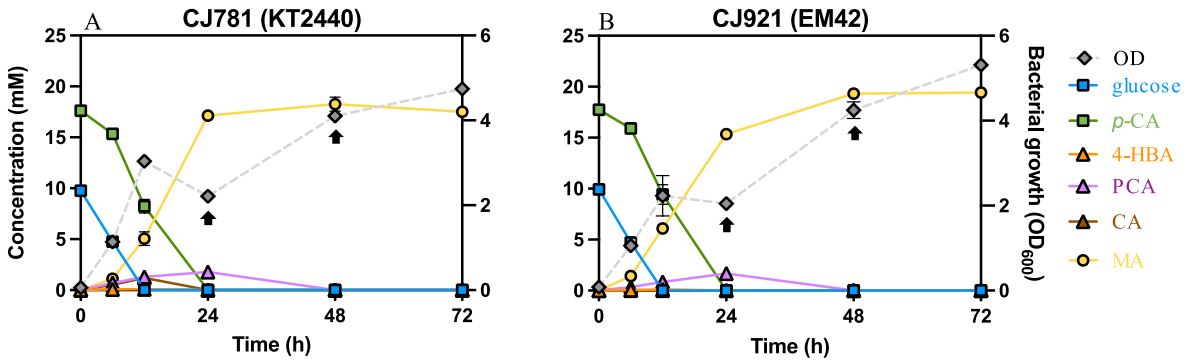

Fig. 2. Shake flask cultivation with *P. putida* KT2440-derived CJ781 and EM42-derived CJ921 for muconate production from *p*-coumarate. (**A**) Shake flask cultivation for *P. putida* KT2440-derived strain CJ781. (**B**) Shake flask cultivation for *P. putida* EM42-derived strain CJ921. Shake flask cultivations were conducted in triplicate in M9 minimal media with 10 mM glucose for growth and 20 mM *p*-CA for conversion to muconate. Samples were taken for OD_{600} measurements and HPLC analysis at 0, 6, 12, 24, 48 and 72 h. At 24 and 48 h, the cultivations were supplemented with 10 mM glucose (indicated with arrows in the graphs). Error bars represent the standard deviation across biological triplicates. Numerical data for this figure are provided in Table S3A.

Table 1
P. putida strains used in this study.

Strain	Genotype	Reference
KT2440	Wild type	
CJ475	Δ*catRBCA*::P_{tac}:*catA* Δ*pcaHG*::P_{tac}:*aroY*:*ecdBD* Δ*crc*	Salvachúa et al. (2018)
CJ680	Δ*catRBCA*::P_{tac}:*catA* Δ*pcaHG*::P_{tac}:*aroY*:*ecdBD* Δ*crc fpvA*:P_{tac}:*praI*:*vanAB*	Kuatsjah et al. (2022)
CJ781	Δ*catRBCA*::P_{tac}:*catA* Δ*pcaHG*::P_{tac}:*aroY*:*ecdBD* Δ*crc* Δ*pobAR fpvA*:P_{tac}:*praI*:*vanAB*	Kuatsjah et al. (2022)
GB062	Δ*catRBCA*::P_{tac}:*catA* Δ*pcaHG*::P_{tac}:*aroY*:*ecdB*:*asbF* Δ*pykA*::P_{tac}:*aroG*-D146N:*aroY*:*ecdB*:*asbF* Δ*pykF* Δ*ppc* Δ*pgi-1* Δ*pgi-2* Δ*gcd* Δ*hexR*	Bentley et al. (2020)
CA042	Δ*catRBCA*::P_{tac}:*catA* Δ*pcaHG*::P_{tac}:*aroY*:*ecdB*:*asbF* Δ*pykA*::P_{tac}:*aroG*-D146N:*aroY*:*ecdB*:*asbF* Δ*pykF* Δ*ppc* Δ*pgi-1* Δ*pgi-2* Δ*gcd* Δ*hexR* Δflagellum	This study
CA115	CA042 Δflagellum::*fabH1*	This study
EM42	KT2440 derivative Δprophages1,2,3,4 ΔTn7 Δ*endA1* Δ*endA2* Δ*hsdRMS* Δflagellum ΔTn*4652*	Martínez-García et al., 2014
CJ916	EM42 Δ*catRBCA*::P_{tac}:*catA* Δ*pcaHG*::P_{tac}:*aroY*:*ecdBD* Δ*crc*	This study
CJ917	EM42 Δ*catRBCA*::P_{tac}:*catA* Δ*pcaHG*::P_{tac}:*aroY*:*ecdBD* Δ*crc fpvA*:P_{tac}:*praI*:*vanAB*	This study
CJ921	EM42 Δ*catRBCA*::P_{tac}:*catA* Δ*pcaHG*::P_{tac}:*aroY*:*ecdBD* Δ*crc* Δ*pobAR fpvA*::P_{tac}:*praI*:*vanAB*	This study
CA055	EM42 Δ*catRBCA*::P_{tac}:*catA* Δ*pcaHG*::P_{tac}:*aroY*:*ecdB*:*asbF* Δ*pykA*:P_{tac}:*aroG*-D146N:*aroY*:*ecdB*:*asbF* Δ*pykF* Δ*ppc* Δ*pgi-1* Δ*pgi-2* Δ*gcd* Δ*hexR*	This study
CA114	EM42 Δflagellum::*fabH1*	This study
CA116	CA055 (EM42 derivative) Δflagellum::*fabH1*	This study
CA117	CJ921 (EM42 derivative) Δflagellum::*fabH1*	This study

had a maximum OD_{600} of 4.7 ± 0.2 while CJ475 reached an OD_{600} of 3.8 ± 1.2. CJ916 also reached a higher concentration of muconate at 48 h compared to CJ475, 14 ± 0.4 mM and 11 ± 1.2 mM, respectively (Figs. S1A–B). CJ917 (expressing *pobAR* and *praI*) did not show improvement compared to the equivalent KT2440 strain CJ680 (Figs. S1C–D, Table S3A). Together, these data suggest that EM42-derived strains do not outperform KT2440-derived strains, with the exception of CJ916 (*pobAR*), in shake flask cultivations for the production of muconate from *p*-coumarate.

3.2. EM42-derived strain CJ921 does not outperform KT2440-derived strain CJ781 for the production of muconate from p-coumarate in bioreactor cultivations

Since the differences observed between CJ781 (KT2440-derived) and CJ921 (EM42-derived) in shake flask cultivations were not significant, we sought to evaluate CJ781 and CJ921 in bioreactors in fed-batch mode, where differences might be amplified (Fig. 3A–B, Table S3B). *p*-Coumarate and glucose, at a ratio of 2:1 (mol:mol), were fed at the same feeding rates in all the bioreactors (5 mmol *p*-coumarate/L/h). Bacterial growth and maximum cell density were similar between strains, excluding the last time point where CJ921 cell density decreased likely due to the accumulation of substrates, which can become toxic. CJ921 and CJ781 had similar titers at 80 h, 37 ± 0.01 g/L, and 38 ± 1 g/L, respectively (Fig. 3A–B). After 80 h the cultivation of CJ921 began to accumulate *p*-coumarate and glucose after 80 h. CJ781 did not accumulate *p*-coumarate or glucose and continued producing muconate for a longer period of time (100 h) (Fig. 3A–B). CJ781 reached a final muconate titer of 45 ± 0.1 g/L after 100 h, while CJ921 reached a final muconate titer of 37 ± 2 g/L after 96 h (Fig. 3A–B).

Because these cultivation conditions did not reveal improvements in the EM42 background compared to KT2440, we changed the ratio between *p*-coumarate and glucose to 8:1 (mol:mol). This modification was based on previous literature that reported that energetic requirements in EM42 are lower than those in KT2440 and biomass yields from glucose are higher in EM42 than KT2440 (Martínez-García et al., 2014a). Thus, we hypothesized that CJ921 may require less glucose for growth and production of muconate compared to CJ781 (Martínez-García et al., 2014a). At a ratio of 8:1, bacterial growth was again similar between strains. CJ921 reached a muconate titer of 31 ± 0.1 g/L, while CJ781 reached a higher muconate titer of 35 ± 2 g/L after 85 h (Fig. 3C–D). At the final time point for the cultivation CJ781 had reached a higher muconate titer compared to CJ921, 40 ± 1 g/L and 32 ± 1 g/L, respectively (Fig. 3C–D). This difference results from greater accumulation of *p*-coumarate at the end of the cultivation for CJ921 compared to CJ781. Overall, these results indicate that the EM42-derived strain does not provide a benefit in our current bioprocess configuration for production of muconate from aromatic compounds.

3.3. EM42-derived strains do not show improved muconate production from glucose compared to KT2440-derived strains in shake flasks

Next, we constructed an EM42-derived strain (CA055) equivalent to a KT2440-derived strain (GB062) (Bentley et al., 2020) engineered to produce muconate from glucose (Fig. 1B) and compared these strains in shake flask cultivations (Fig. 4, Table S3C). GB062 reached a maximum OD_{600} of 2 at 48 h, while CA055 did not reach the same OD_{600} until 72 h (Fig. 4). Although, both GB062 and CA055 ultimately produced equivalent amounts of muconate (10 mM), GB062 made muconate significantly faster (48 h) compared to CA055 (72 h) (Fig. 4).

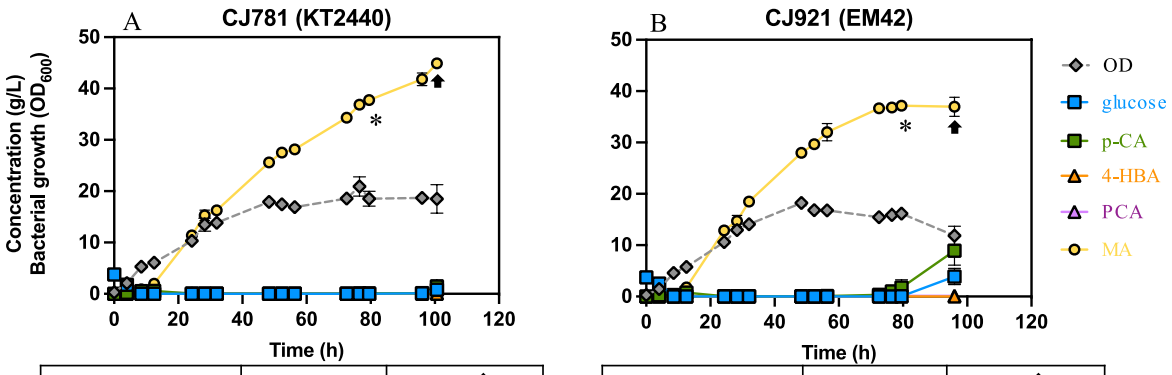

Time (h)	80 (*)	100 (↑)
Titer (g/L)	38 ± 1	45 ± 0.1
Yield (mol/mol)	1.02 ± 0.002	1.00 ± 0.01
Productivity (g/L/h)	0.47 ± 0.01	0.45 ± 0.001

Time (h)	80 (*)	96 (↑)
Titer (g/L)	37 ± 0.01	37 ± 2
Yield (mol/mol)	0.97 ± 0.03	0.86 ± 0.07
Productivity (g/L/h)	0.47 ± 0.0001	0.38 ± 0.02

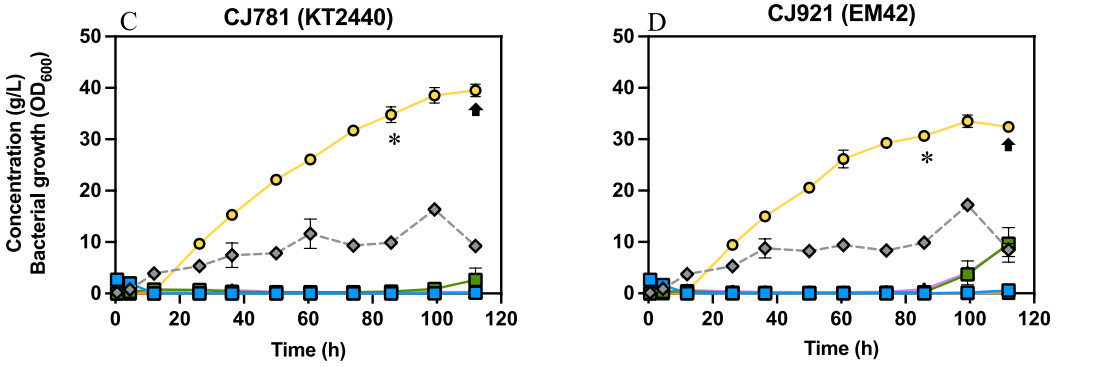

Time (h)	85 (*)	112 (↑)
Titer (g/L)	35 ± 2	40 ± 1
Yield (mol/mol)	1.11 ± 0.04	1.06 ± 0.04
Productivity (g/L/h)	0.43 ± 0.003	0.39 ± 0.02

Time (h)	85 (*)	112 (↑)
Titer (g/L)	31 ± 0.1	32 ± 1
Yield (mol/mol)	1.01 ± 0.04	0.86 ± 0.03
Productivity (g/L/h)	0.40 ± 0.00	0.34 ± 0.01

Fig. 3. Muconate production by CJ781 and CJ921 in bioreactors with varying ratios of *p*-coumarate to glucose. (**A**) Bioreactor profile for *P. putida* strain CJ781 (KT2440-derived) with a *p*-coumarate to glucose molar ratio of 2:1. (**B**) Bioreactor profile for *P. putida* strain CJ921 (EM42-derived) with a *p*-coumarate to glucose molar ratio of 2:1. (**C**) Bioreactor profile for *P. putida* strain CJ781 (KT2440-derived) with a *p*-coumarate to glucose molar ratio of 8:1. (**D**) Bioreactor profile for *P. putida* strain CJ921 (EM42-derived) with a *p*-coumarate to glucose molar ratio of 8:1. Muconate titers, yields, and productivities shown in the table were calculated before *p*-coumarate accumulated during the fermentations (highlighted with an * in the graphs) as well as for the final time point of the fermentations (indicated with an arrow in the graphs). Error bars represent the absolute difference between biological duplicates. Graphs show cell growth and metabolite concentration in the bioreactors during the cultivation. Numerical data for this figure are provided in Table S3B.

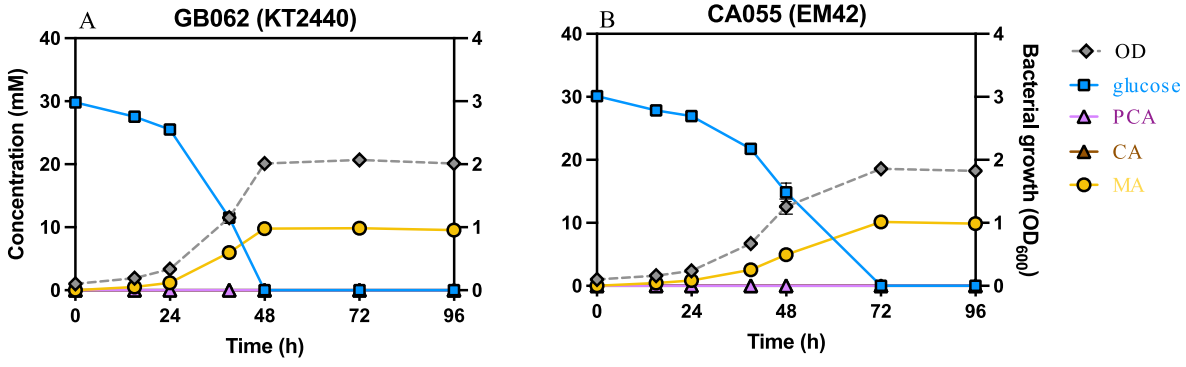

Fig. 4. Shake flask cultivations to compare *P. putida* KT2440-derived strain GB062 and EM42-derived strain CA055 for muconate production from glucose. (**A**) Shake flask cultivation for KT2440-derived strain GB062. (**B**) Shake flask cultivation for EM42-derived strain CA055. The cultivations were conducted in triplicate in M9 minimal media with 30 mM glucose for growth and conversion to muconate. Samples were taken for OD_{600} and HPLC analysis at 0, 6, 12, 24, 48, 72 and 96 h. Error bars represent the standard deviation across biological triplicates. Numerical data for this figure are provided in Table S3C.

3.4. EM42-derived strain CA055 does not outperform KT2440-derived strain GB062 for the production of muconate from glucose in bioreactor cultivations

Although CA055 (EM42-derived) did not exhibit improved muconate productivity in shake flask cultivations compared to GB062 (KT2440-derived), we sought to evaluate these strains in bioreactors in fed-batch mode. The starting concentration of glucose in the bioreactors was 25 g/L. Feeding of glucose began when the glucose concentration in the bioreactors was <10 g/L and the feeding rate was manually adjusted to maintain glucose concentration between 1 and 10 g/L in the bioreactors (Fig. S2). GB062 reached a maximum OD_{600} of 13.5 ± 0.4 while CA055 reached a maximum OD_{600} of 9.7 ± 0.4 (Fig. 5). Overall, GB062 utilized more glucose (80 ± 3 g/L) compared to CA055 (49 ± 3 g/L). GB062 reached a muconate titer of 20 ± 0.4 g/L at a productivity of 0.17 ± 0.01 at 120 h, while CA055 reached a muconate titer of 13 ± 0.3 g/L at a productivity of 0.11 ± 0.01. These results demonstrate that the EM42 background does not improve the production of muconate from glucose in our current bioprocess configuration.

3.5. Genome resequencing of CA055 and CJ921 did not reveal mutations that would significantly affect the strain performance

To confirm that the differential phenotypes observed between the EM42-derived production strains (CA055 and CJ921) and the KT2440-derived production strains (GB062 and CJ781) were not caused by mutations in the strains, we performed genome resequencing. When genome resequencing for CA055 (EM42-derived) and GB062 (KT2440-derived) were compared, 10 single nucleotide polymorphisms (SNPs) and polymorphisms were identified between the strains, none of which would likely alter strain performance or phenotype (Table S4). When genome resequencing for CJ921 (EM42-derived) was compared to CJ781 (KT2440-derived), 13 SNPs and polymorphisms were identified between the strains, also none of which would be predicted to alter strain performance or phenotype (Table S4). Genome resequencing of CA055 and CJ921 did not identify mutations that would have a clear impact on strain performance.

3.6. Reintroduction of FabH1 does not improve production of muconate from p-coumarate or glucose

When examining the genes deleted during the generation of EM42, we noticed that *fabH1* (PP_4379) was deleted along with the fragment of the genome encoding the flagellum (Martínez-García et al., 2014a). FabH1 is involved in fatty acid biosynthesis and has been demonstrated to be important in both *E. coli* and *B. subtilis* (Choi et al., 2000; McNaught et al., 2023). Although *fabH1* is redundant in *P. putida* and its deletion does not markedly affect growth of an otherwise WT strain on glucose, we hypothesized that loss of *fabH1* may be detrimental in production strains (McNaught et al., 2023). To evaluate this, we reintroduced *fabH1* under the control of its native promoter and terminator where the genes encoding the flagellum were deleted. We evaluated CA117 (CJ921 with Δflagellum::*fabH1*) in shake flask cultivations for the production of muconate from *p*-coumarate, compared to CJ921 (Table 1, Figure S3A-B, Table S3E). Reintroduction of *fabH1* did not exhibit any benefit in shake flask cultivations when CA117 was compared to CJ921 (Figs. S3A–B). We also sought to determine if *fabH1* would improve production of muconate from glucose by reintroducing *fabH1* into CA055 to generate CA116 and evaluating these strains in shake flask cultivations (Table 1, Figs. S3C–D, Table S3E). CA055 and CA116 reached equivalent OD_{600} and muconate concentrations after 48 h. Together these results suggest that deletion of *fabH1* does not affect performance of these strains.

3.7. Deletion of the flagellar machinery alone does not improve production of muconate from glucose

Since the EM42-derived strains did not exhibit improvements relative to the KT2440-derived strains, we sought to determine if deletion of only the genes responsible for the flagellum was beneficial in absence of the other deletions included in EM42. We deleted a fragment of the genome containing these genes in GB062 to generate CA042 (Table 1). We then evaluated GB062 and CA042 in shake flask cultivations but observed no significant differences in growth or production of muconate between GB062 and CA042 (Fig. S4, Table S2C). Interestingly, CA042 performed better than CA055, the equivalent EM42-derived strain (Fig. S4, Fig. 4). CA042 reached a maximum OD_{600} and produced 10 mM of muconate by 48 h, while it took CA055 72 h. Although reintroduction of *fabH1* did not improve muconate production from glucose in CA055, we reintroduced *fabH1* in CA042 to generate CA115 (Table 1, Fig. S5, Table S3E). Reintroduction of *fabH1* did not show any benefit in this context either.

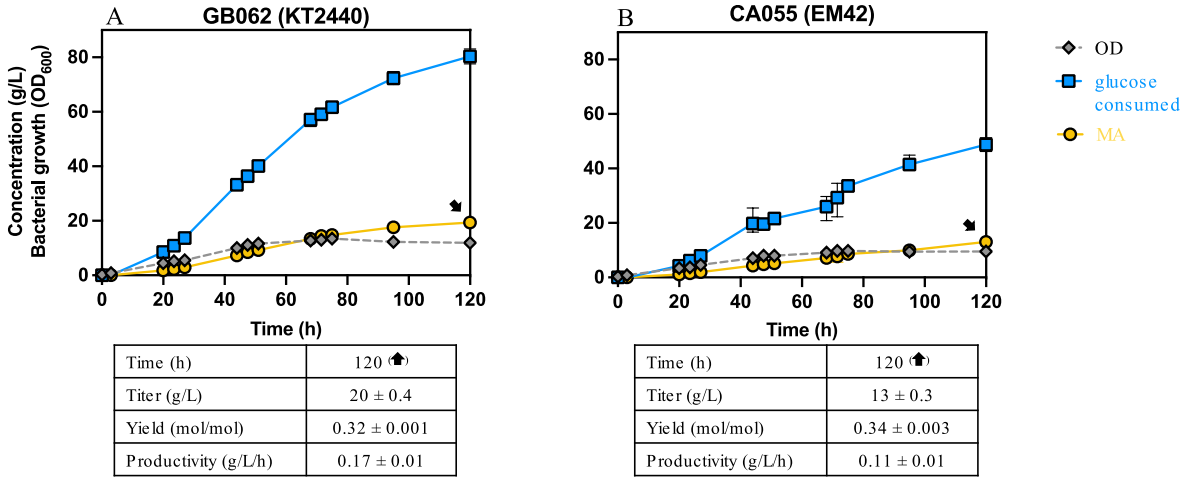

Time (h)	120
Titer (g/L)	20 ± 0.4
Yield (mol/mol)	0.32 ± 0.001
Productivity (g/L/h)	0.17 ± 0.01

Time (h)	120
Titer (g/L)	13 ± 0.3
Yield (mol/mol)	0.34 ± 0.003
Productivity (g/L/h)	0.11 ± 0.01

Fig. 5. Bioreactor cultivations to compare KT2440-derived strain GB062 and EM42-derived strain CA055 for muconate production from glucose. (**A**) Bioreactor profile for GB062 (KT2440-derived). (**B**) Bioreactor profile for CA055 (EM42-derived). The blue line represents glucose that was utilized over time. Muconate titers, yields, and productivities shown in the table were calculated for the final time point of the fermentations (indicated with an arrow in the graphs). Error bars represent the absolute difference across biological duplicates. Numerical data for this figure are provided in Table S3D.

3.8. EM42 exhibits a slower growth rate than KT2440 when aromatic compounds are the sole carbon source

We next sought to understand why the EM42-derived strains did not outperform the equivalent KT2440-derived strains in our experiments. Previous work has shown that EM42 has reduced lag and increased growth rate on glucose, as well as glucose and aromatic compounds together (Martínez-García et al., 2014a; Kohlstedt et al., 2022) but growth on aromatic compounds at the sole carbon source has not been evaluated. Since the production strains CJ781 and CJ921 cannot grow on aromatic compounds as the sole carbon source we utilized EM42 and KT2440 to evaluate growth on various aromatic substrates in plate reader experiments (Fig. 6, Fig. S6, Tables S3F–G). We also evaluated restoration of *fabH1* in EM42 (CA114) (Table 1, Fig. S6). Interestingly, there were some aromatic substrates that CA114 grew marginally better on than EM42, but there was no difference between CA114 and EM42 when grown on glucose (Fig. S6). In line with previous work, EM42, and CA114, exhibited no lag on the aromatic compounds evaluated (Fig. S6) but the growth of the EM42 was initially linear prior to becoming exponential (Fig. S6). Despite the lag being shorter for EM42, we observed that KT2440 grew significantly faster on the aromatics evaluated, with the exception of 10 mM vanillate and 5 mM catechol (Fig. S6, Fig. 6A–B). In addition to differences in growth rate, we observed differences in biomass accumulation between KT2440 and EM42 (Fig. S6, Fig. 6C–D); At lower concentrations of aromatic compounds, EM42 reached higher maximum biomass accumulation, but at high concentrations of aromatic compounds, with the exception of protocatechuate and catechol, KT2440 reached higher maximum biomass yields (Fig. 6C–D).

3.9. EM42 production strains exhibit superior growth on lower concentrations of glucose but the benefit is diminished on higher concentrations of glucose

Previous work has shown that EM42 has reduced lag and increased growth rate on glucose compared to KT2440 (Martínez-García et al., 2014a). To compare the growth of our production strains on glucose (in the absence of muconate production), we utilized plate reader cultivations. We observed that the EM42-derived production strain CJ921 had a shorter lag and grew to a higher OD_{600} than the equivalent

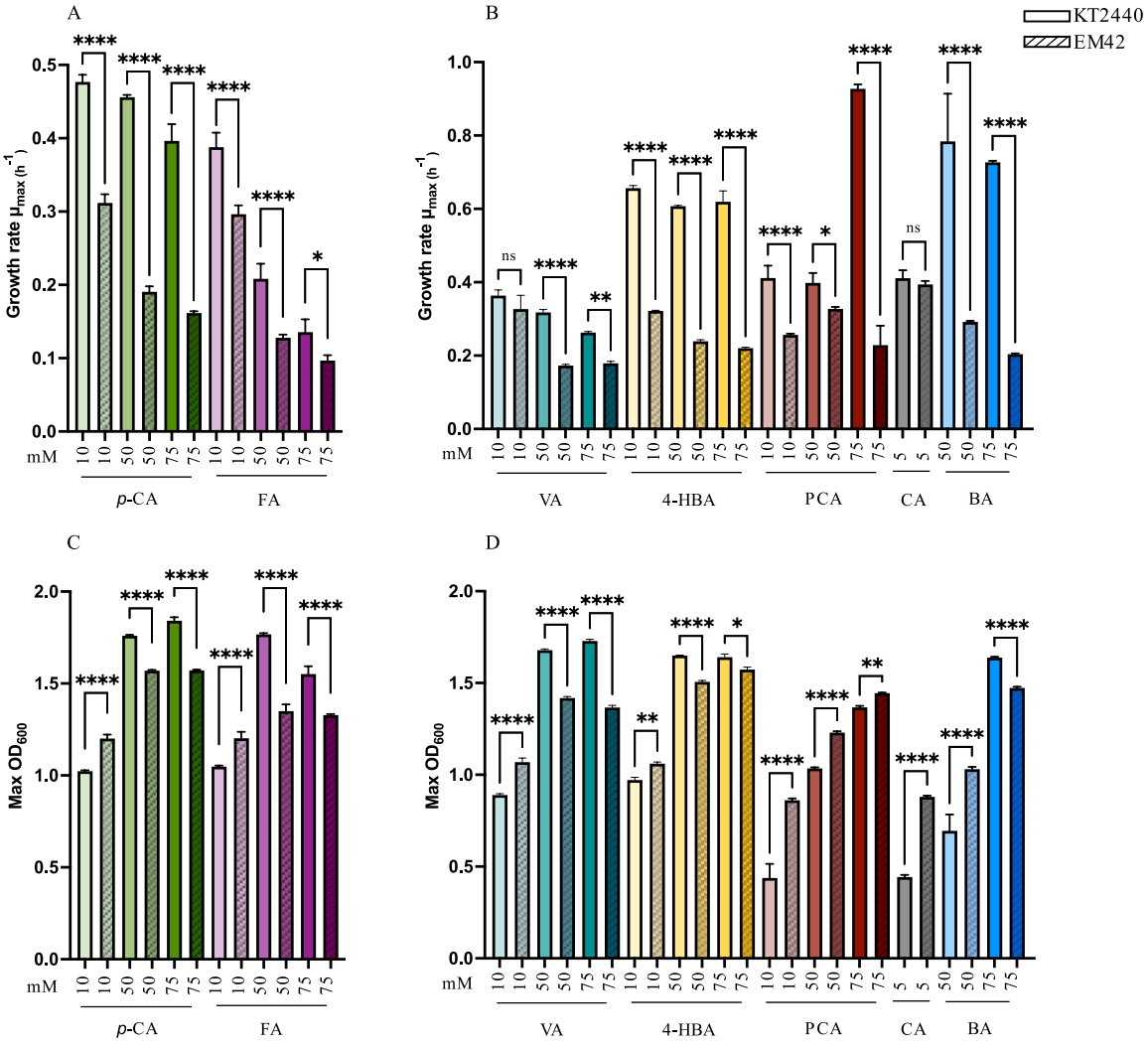

Fig. 6. Plate reader cultivations to compare growth of *P. putida* strains KT2440 and EM42 on aromatic compounds. (**A**) Growth rates of *P. putida* KT2440 and EM42 on either FA or *p*-CA at three different concentrations. (**B**) Growth rates of *P. putida* KT2440 and EM42 on 4-HBA, VA, PCA, CA or BA. (**C**) Maximum OD_{600} of *P. putida* KT2440 and EM42 on either FA or *p*-CA at three different concentrations. (**D**) Maximum OD_{600} of *P. putida* KT2440 and EM42 on 4-HBA, VA, PCA, CA or BA. The error bars represent the standard deviation of three biological replicates. Abbreviations: *p*-CA; *p*-coumarate, FA; ferulate, 4-HBA; 4-hydroxybenzoate, VA; vanillate, PCA; protocatechuate, CA; catechol, BA; benzoate. Statistics: ****P < 0.0001, ***P < 0.0005, **P < 0.005, *P < 0.05, NS not significant. Numerical data for this figure are provided in Table S3G.

KT2440-derived strain CJ781 on 10 mM glucose when no aromatic compound was present (Fig. S7, Table S3H). However, when the concentration of glucose was increased to 30 mM glucose without aromatic compounds, CJ781 and CJ921 grew more similarly; specifically, CJ781 still exhibited a longer lag than CJ921 but both strains reached an equivalent maximum OD_{600} (Fig. S7). We also observed that the EM42-derived production strain CA055 had a shorter lag and grew to a higher OD_{600} compared to the KT2440-derived equivalent GB062 when grown on 10 mM glucose (Fig. S7, Table S3G). Consistent with our shake flask cultivations, on 30 mM glucose, GB062 grew faster and reached a maximum OD earlier in the cultivation than the equivalent EM42-derived strain CA055 (Fig. S7). Both CA055 and GB062 exhibited similar growth lags of ~24 h and grew to a similar maximum OD_{600} (~1.27), but GB062 reached its maximum OD_{600} after ~48 h, while it took CA055 72 h to reach the same OD_{600} (Fig. S7).

3.10. EM42 strains have altered gene expression relative to KT2440 strains

To further understand the differences between EM42 and KT2440 *P. putida* strains, we performed transcriptomics analysis. We first compared gene expression in EM42 and KT2440 when grown on *p*-CA. We used the original strains rather than the production strains to avoid any confounding effects of glucose, which is required for the production strains to grow. Principal component analysis showed strong separation between EM42 and KT2440 (Fig. S8A). When grown on 50 mM *p*-CA, there were 210 genes (excluding the genes known to be deleted in EM42) with significant differential expression in EM42 relative to KT2440 ($p < 0.05$ and $\log_2$ fold-change (>|1|) (Fig. 7A, Fig. S9A, Table S3I). There were three genes related to aromatic catabolism that had significant differences in abundance, PP_2643 (*pcaY*), PP_2035 (*benE-I*) and PP_3713 (*catA1*) (Fig. 7A). The expression of PP_2643 (*pcaY*) was significantly downregulated in EM42 relative KT2440 (Fig. 7A). PP_2643 (*pcaY*) is an aromatic acid chemoreceptor and has been shown to be important for the detection of aromatic compounds in *P. putida* F1 (Luu et al., 2015). PP_2035 (*benE-I*) is annotated as a benzoate transporter. Interestingly, *catA1* which expresses catechol 1, 2-dioxygenase, was significantly upregulated in all the comparisons between KT2440 and EM42 strains (Fig. 7A–C). Increased expression of *catA1* may help explain why EM42 strains have been reported to be more tolerant to catechol (Kohlstedt et al., 2022).

Since production strain CA055 (EM42-derived) performed worse in both flask and bioreactor cultivations than GB062 (KT2440-derived) we sought to compare expression levels between these strains. Principal component analysis showed strong separation between CA055 and GB062 (Figs. S8B-C). When grown on 10 mM glucose, there were 661 genes (excluding the genes known to be deleted in EM42) with significant differential expression in CA055 relative to GB062 ($p < 0.05$ and $\log_2$ fold-change (>|1|) (Fig. 7B, Fig. S9B, Table S3J). Of the 661 genes with differential expression, 68.5% had reduced expression in CA055 relative to GB062. When grown on 30 mM glucose, there were 598 genes (excluding the genes known to be deleted in EM42) with significant differential expression in CA055 relative to GB062 ($p < 0.05$ and $\log_2$ fold-change (>|1|) (Fig. 7C, Fig. S9C, Table S2K). Of the 598 genes with differential expression, 76.5% had reduced expression in CA055 relative to GB062. We expected to observe differential gene expression for

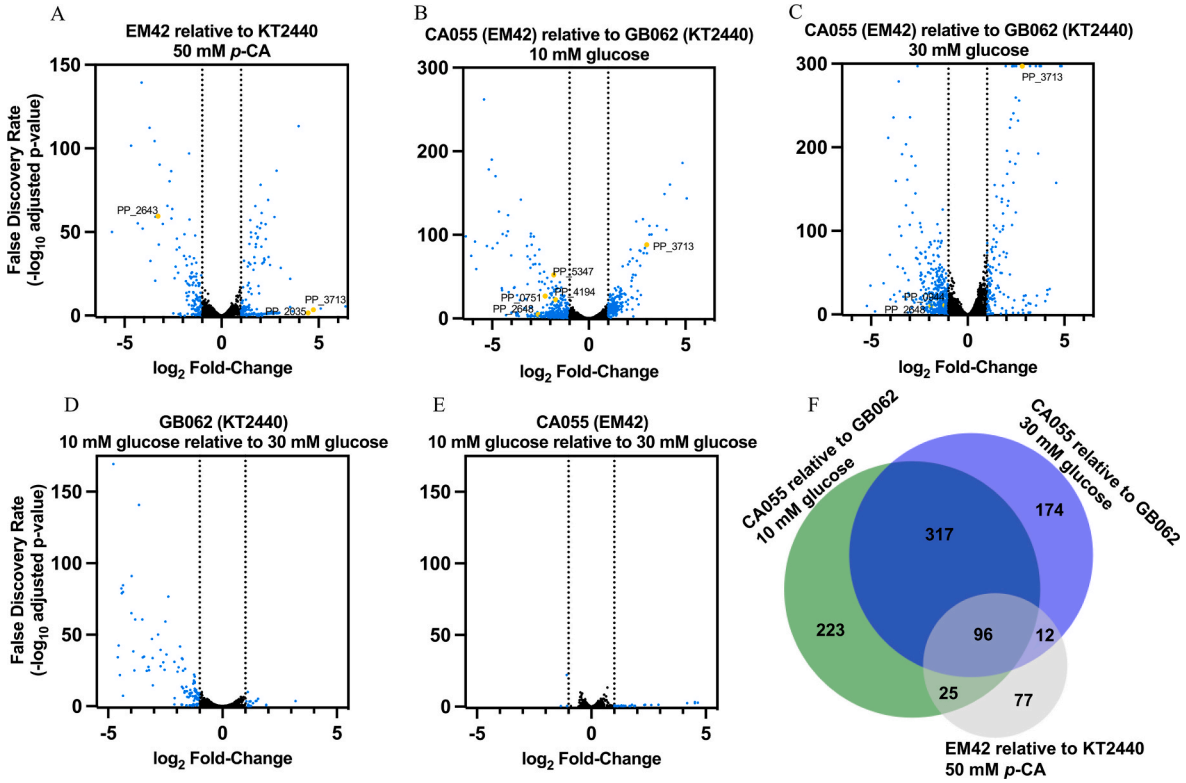

Fig. 7. Transcriptomics analysis to compare gene expression of EM42 and derived strains relative to KT2440 and derived strains. (**A**) Volcano plot showing the comparison of gene expression of EM42 relative to KT2440 on 50 mM *p*-coumarate. (**B**) Volcano plot showing the comparison of gene expression of CA055 (EM42) relative to GB062 (KT2440) on 10 mM glucose. (**C**) Volcano plot showing the comparison of gene expression of CA055 (EM42-derived) relative to GB062 (KT2440-derived) on 30 mM glucose. (**D**) Volcano plot showing the comparison of gene expression of GB062 (KT2440-derived) on 10 mM glucose relative to 30 mM glucose. (**E**) Volcano plot showing the comparison of gene expression of CA055 (EM42-derived) on 10 mM glucose relative to 30 mM glucose. (**F**) Venn diagram for all genes with significant adjusted p-values (<0.05) and $\log_2$ fold-change (>|1|). Genes deleted in EM42 were excluded from the analysis to highlight the effects genome reduction had on transcript levels of present genes. Genes where the adjusted p-value was so small it rounded to zero were assigned the lowest adjusted p-value prior to rounding. Numerical data for this figure are provided in Table S3I-M.

critical genes related to glucose metabolism or growth between CA055 and GB062 but the differences were limited; only 1 and 7 genes showed significant differential expression at 30 mM and at 10 mM glucose, respectively. Interestingly, when grown on 10 mM glucose, CA055 had lower expression than GB062 of multiple genes involved in glucose metabolism or the TCA cycle, including PP_5347 (*pycA*), PP_4194 (*gltA*), and PP_0751 (*mqo1*) despite CA055 growing better on 10 mM glucose (Fig. 7B, Fig. S9B). Interestingly, the universal stress response protein, PP_2684 was expressed at lower levels in CA055 relative to GB062 at both 10 mM and 30 mM glucose (Fig. 7B–C) (Bentley et al., 2020). Reduced gene expression in CA055 relative to GB062 at both glucose concentrations may indicate a global reduction in gene expression in EM42-derived strains.

To better understand how CA055 and GB062 adapted to differences in glucose concentration and, consequently, changes in muconate production, we compared gene expression in GB062 grown on 10 mM glucose relative to 30 mM glucose and CA055 grown on 10 mM glucose relative to 30 mM glucose (Fig. 7D–E, Figs. S8D-E, Table S3L-M). In GB062, there were 110 genes with significant differential expression and the vast majority with decreased expression on 10 mM glucose relative to 30 mM (Fig. 7D). When transcript levels of CA055 growing on 10 mM and 30 mM glucose were compared only 6 genes showed significant differential expression (Fig. 7E). Overall, these results indicate that CA055 does not modulate gene expression to the same degree as GB062 in response to changes in glucose concentration and/or muconate production.

Further analysis revealed genes with differential expression existed in all comparisons regardless of genotype, substrate, or substrate concentration (Fig. 7F). The 96 genes with differential expression across all three evaluated conditions mostly fell into one or more basic categories: genes regulated by or important for the regulation of *fleQ* (regulator of flagellar genes), genes involved in chemotaxis, and/or hypothetical proteins with unknown function. Together, these results underscore that genome reduction causes significant changes in overall gene expression.

4. Discussion

In this work, we compared *P. putida* KT2440- and EM42-derived strains engineered for muconate production from either *p*-coumarate or glucose to determine if previously described benefits (reduced growth lag phase, improved biomass yield, increased intracellular ATP, and intracellular NADPH ratios) associated with genome reduction in EM42 might improve strain performance (Martínez-García et al., 2014a; Martínez-García et al., 2014b). Although genome reduction in KT2440 has yielded benefits in previous studies (Martínez-García et al., 2014a; Martínez-García et al., 2014b), this work identified conditions wherein genome reduction is not beneficial to producing muconic acid from two substrates. It is important to note that this finding suggests, when use of EM42 is of interest, that there is value in comparing the wild-type KT2440 strain and EM42 (or generally, parental strains and genome-reduced strains) in the context that they are intended to be used.

For muconate production from *p*-coumarate, our results show that EM42-derived strains do not outperform KT2440-derived strains in shake flasks or bioreactors (Figs. 2 and 3), likely because EM42 exhibits lower growth rates on most aromatic compounds and is less tolerant to aromatic compounds (Figs. 6 and 7). There was one exception to this observation, in shake flasks CJ916 (EM42-derived) reached a higher max OD_{600} (4.7 ± 0.2) compared to the equivalent KT2440-derived strain, CJ475 (OD_{600} 3.8 ± 1.2) when grown on 10 mM glucose. By 48 hours, CJ916 also reached a higher concentration of muconate from *p*-coumarate compared to CJ475, 14 ± 0.4 mM and 11 ± 1.2 mM, respectively (Figs. S1A–B). CJ475 and CJ916 rely on PobA which requires NADPH and may cause NADPH to be limited (Kuatsjah et al., 2022). This highlights that EM42-derived strains may have the advantage in conditions where NADPH is limiting due to the improved NADPH/NADP + ratios (Martínez-García et al., 2014a).

Although we observed improved growth on glucose for EM42-derived CJ921 on lower concentrations of glucose (10 mM) compared to KT2440-derived CJ781, the benefits were negated in conditions where aromatic compounds are present, resulting in similar growth between the two strains (Figs 2 and S7). Interestingly, EM42 had a shorter lag phase compared to KT2440 for growth on aromatic compounds (Fig. S6), suggesting that EM42 should be considered as a production strain relative to KT2440 when attempting to overcome conditions with long lag phases or that require high concentration of aromatic compounds during the cultivations.

Similarly, we also observed that EM42 does not outperform KT2440 in shake flasks or bioreactors for muconate production from glucose (Figs. 4 and 5). Although EM42 exhibits superior growth on glucose (Martínez-García et al., 2014a), we observed that when the glucose concentration is increased from 10 mM to 30 mM, the benefits are diminished (Fig. S6). Based on the transcriptomics data presented here, we hypothesize that this observation is related to changes in gene expression resulting from genome reduction (Fig. 7). We observed that the EM42-derived production strain CA055 displayed a global reduction in gene expression relative to GB062 (Fig. 7B–C) and did not substantially alter gene expression in response to changes in glucose concentration as was observed in the KT2440-derived equivalent (Fig. 7D–E), which may explain why EM42-derived CA055 performs more poorly than the equivalent KT2440-derived strain GB062 in both shake flask and bioreactor cultivations. The large changes in gene expression we observed highlight the potential pleotropic effects of removing portions of the genome and deleting regulators.

Although our results agree with previous findings that genome reduction is not universally beneficial (Kurokawa et al., 2016; Calvey et al., 2023), it can still be a useful strategy for improving bacterial hosts and will continue to be used in microbial hosts to improve growth, production, tolerance, genetic tractability, and other beneficial phenotypes (Pósfai et al., 2013; Lee et al., 2009; Suárez et al., 2019; Yan et al., 2018; Zhang et al., 2020). Since *P. putida* EM42 was shown to exhibit improved characteristics compared to KT2440, many publications have successfully utilized EM42 to produce PHAs, catabolize a variety of compounds, and produce industrially relevant compounds such as muconate or propionate (Cha et al., 2020; Dvořák, P and de Lorenzo, 2018; Dvořák et al., 2020a; Dvořák et al., 2020b; García-Hidalgo et al., 2019; Kohlstedt et al., 2022; Tiwari et al., 2022; Turlin et al., 2022). Taken together, these publications highlight the popularity and usefulness of genome-reduced *P. putida* strains, with the work here suggesting that production strains derived from KT2440 and EM42 should be directly compared, and that further understanding of the effects of genome reduction in *P. putida* KT2440 will be useful to *a priori* select a base strain for metabolic engineering.

Author statement

Caroline R. Amendola: conceptualization, formal analysis, investigation, writing – original draft, writing – review & editing. William T. Cordell: investigation, writing – review & editing. Colin M. Kneucker: investigation. Caralyn J. Szostkiewicz: investigation. Morgan A. Ingraham: investigation. Michela Monninger: investigation. Rosemarie Wilton: investigation. Brian F. Pfleger: writing – review & editing, supervision. Davinia Salvachúa: conceptualization, writing – original draft, writing – review & editing, supervision, funding acquisition. Christopher W. Johnson: conceptualization, writing – original draft, writing – review & editing, supervision, funding acquisition. Gregg T. Beckham: conceptualization, writing – original draft, writing – review & editing, supervision, funding acquisition.

Data availability

All data in figures are available in the Supplemental Information file.

The sequencing data are uploaded to NCBI as noted in the Data Availability statement.

Acknowledgements

This work was authored in part by Alliance for Sustainable Energy, LLC, the manager and operator of the National Renewable Energy Laboratory for the U.S. Department of Energy (DOE) under Contract No. DE-AC36-08GO28308. Funding was provided by the U.S. Department of Energy Office of Energy Efficiency and Renewable Energy Bioenergy Technologies Office (BETO), including partly from the Agile BioFoundry. This material is also partially based upon work supported by the U.S. Department of Energy, Office of Science, Office of Workforce Development for Teachers and Scientists, Office of Science Graduate Student Research (SCGSR) program to WTC. The SCGSR program is administered by the Oak Ridge Institute for Science and Education for the DOE under contract number DE-SC0014664.

We thank Kevin J. McNaught and W. Ray Henson for bringing to our attention the *fabH1* deletion in EM42, Chen Ling for suggesting that we conduct transcriptomics experiments, Allison Yaguchi for input on transcriptomics analysis, Esteban Martínez-García and Víctor de Lorenzo for providing us with the *P. putida* EM42 strain, Victor de Lorenzo for helpful discussions, Allison Z. Werner and Peter C. St. John for help with Fig. 1, and Stefan Haugen and Alexander F. Benson for assisting with the HPLC analysis.

Appendix A. Supplementary data

Supplementary data to this article can be found online at https://doi.org/10.1016/j.ymben.2023.11.004.

References

Almqvist, H., Veras, H., Li, K., Garcia Hidalgo, J., Hulteberg, C., Gorwa-Grauslund, M., Skorupa Parachin, N., Carlquist, M., 2021. Muconic acid production using engineered *Pseudomonas putida* KT2440 and a guaiacol-rich fraction derived from kraft lignin. ACS Sustain. Chem. Eng. 9 (24), 8097–8106.

Aparicio, T., de Lorenzo, V., Martínez-García, E., 2019. Improved thermotolerance of genome-reduced *Pseudomonas putida* EM42 enables effective functioning of the P_L/cI857 system. Biotechnol. J. 14 (1).

Ara, K., Ozaki, K., Nakamura, K., Yamane, K., Sekiguchi, J., Ogasawara, N., 2007. *Bacillus* minimum genome factory: effective utilization of microbial genome information. Biotechnol. Appl. Biochem. 46 (3), 169–178.

Bentley, G.J., Narayanan, N., Jha, R.K., Salvachúa, D., Elmore, J.R., Peabody, G.L., Black, B.A., Ramirez, K., De Capite, A., Michener, W.E., Werner, A.Z., Klingeman, D. M., Schindel, H.S., Nelson, R., Foust, L., Guss, A.M., Dale, T., Johnson, C.W., Beckham, G.T., 2020. Engineering glucose metabolism for enhanced muconic acid production in *Pseudomonas putida* KT2440. Metab. Eng. 59, 64–75.

Bleem, A., Kuatsjah, E., Presley, G.N., Hinchen, D.J., Zahn, M., Garcia, D.C., Michener, W.E., König, G., Tornesakis, K., Allemann, M.N., Giannone, R.J., McGeehan, J.E., Beckham, G.T., Michener, J.K., 2022. Discovery, characterization, and metabolic engineering of Rieske non-heme iron monooxygenases for guaiacol *O*-demethylation. Chem Catal. 2 (8), 1989–2011. https://doi.org/10.1016/j.checat.2022.04.019.

Calvey, C.H., Sànchez i Nogué, V., White, A.M., Kneucker, C.M., Woodworth, S.P., Alt, H. M., Eckert, C.A., Johnson, C.W., 2023. Improving growth of *Cupriavidus necator* H16 on formate using adaptive laboratory evolution-informed engineering. Metab. Eng. 75, 78–90. October 2022.

Cha, D., Ha, H.S., Lee, S.K., 2020. Metabolic engineering of *Pseudomonas putida* for the production of various types of short-chain-length polyhydroxyalkanoates from levulinic acid. Bioresour. Technol. 309 (April), 123332.

Chen, S., Zhou, Y., Chen, Y., Gu, J., 2018. Fastp: an ultra-fast all-in-one FASTQ preprocessor. Bioinformatics 34 (17), i884–i890.

Choe, D., Cho, S., Kim, S.C., Cho, B.K., 2016. Minimal genome: worthwhile or worthless efforts toward being smaller? Biotechnol. J. 11 (2), 199–211.

Choi, K.H., Heath, R.J., Rock, C.O., 2000. β-ketoacyl-acyl carrier protein synthase III (FabH) is a determining factor in branched-chain fatty acid biosynthesis. J. Bacteriol. 182 (2), 365–370.

Choi, K.H., Kumar, A., Schweizer, H.P., 2006. A 10-min method for preparation of highly electrocompetent *Pseudomonas aeruginosa* cells: application for DNA fragment transfer between chromosomes and plasmid transformation. J. Microbiol. Methods 64 (3), 391–397.

Cywar, R.M., Rorrer, N.A., Hoyt, C.B., Beckham, G.T., Chen, E.Y.X., 2022. Bio-based polymers with performance-advantaged properties. Nat. Rev. Mater. 7 (2), 83–103.

Draths, K.M., Frost, J.W., 1994. Environmentally compatible synthesis of adipic acid from o-glucose. J. Am. Chem. Soc. 10, 399–400.

Dvořák, P., de Lorenzo, V., 2018. Refactoring the upper sugar metabolism of *Pseudomonas putida* for co-utilization of cellobiose, xylose, and glucose. Metab. Eng. 48, 94–108. June.

Dvořák, P., Bayer, E.A., De Lorenzo, V., 2020a. Surface display of designer protein scaffolds on genome-reduced strains of *Pseudomonas putida*. ACS Synth. Biol. 9 (10), 2749–2764.

Dvořák, P., Kováč, J., de Lorenzo, V., 2020b. Biotransformation of d-xylose to d-xylonate coupled to medium-chain-length polyhydroxyalkanoate production in cellobiose-grown *Pseudomonas putida* EM42. Microb. Biotechnol. 13 (4), 1273–1283.

Fan, X., Zhang, Y., Zhao, F., Liu, Y., Zhao, Y., Wang, S., Liu, R., Yang, C., 2020. Genome reduction enhances production of polyhydroxyalkanoate and alginate oligosaccharide in *Pseudomonas mendocina*. Int. J. Biol. Macromol. 163, 2023–2031, 2020.

García-Hidalgo, J., Ravi, K., Kuré, L.L., Lidén, G., Gorwa-Grauslund, M., 2019. Identification of the two-component guaiacol demethylase system from Rhodococcus rhodochrous and expression in *Pseudomonas putida* EM42 for guaiacol assimilation. Amb. Express 9 (1).

Giga-Hama, Y., Tohda, H., Takegawa, K., Kumagai, H., 2007. *Schizosaccharomyces pombe* minimum genome factory. Biotechnol. Appl. Biochem. 46 (3), 147–155.

Hashimoto, M., Ichimura, T., Mizoguchi, H., Tanaka, K., Fujimitsu, K., Keyamura, K., Ote, T., Yamakawa, T., Yamazaki, Y., Mori, H., Katayama, T., Kato, J.I., 2005. Cell size and nucleoid organization of engineered *Escherichia coli* cells with a reduced genome. Mol. Microbiol. 55 (1), 137–149.

Hemmerich, J., Labib, M., Steffens, C., Reich, S.J., Weiske, M., Baumgart, M., Rückert, C., Ruwe, M., Siebert, D., Wendisch, V.F., Kalinowski, J., Wiechert, W., Oldiges, M., 2020. Screening of a genome-reduced *Corynebacterium glutamicum* strain library for improved heterologous cutinase secretion. Microb. Biotechnol. 13 (6), 2020–2031.

Henson, W.R., Meyers, A.W., Jayakody, L.N., DeCapite, A., Black, B.A., Michener, W.E., Johnson, C.W., Beckham, G.T., 2021. Biological upgrading of pyrolysis-derived wastewater: engineering *Pseudomonas putida* for alkylphenol, furfural, and acetone catabolism and (methyl)muconic acid production. Metab. Eng. 68, 14–25. July.

Hulsen, T., 2022. DeepVenn – a Web Application for the Creation of Area-Proportional Venn Diagrams Using the Deep Learning Framework Tensorflow.Js. Posted on aRXiv on September 27th, 2022.

Jayakody, L.N., Johnson, C.W., Whitham, J.M., Giannone, R.J., Black, B.A., Cleveland, N. S., Klingeman, D.M., Michener, W.E., Olstad, J.L., Vardon, D.R., Brown, R.C., Brown, S.D., Hettich, R.L., Guss, A.M., Beckham, G.T., 2018. Thermochemical wastewater valorization: via enhanced microbial toxicity tolerance. Energy Environ. Sci. 11 (6), 1625–1638.

Jiménez, J.I., Miñambres, B., García, J.L., Díaz, E., 2002. Genomic analysis of the aromatic catabolic pathways from *Pseudomonas putida* KT2440. Environ. Microbiol. 4 (12), 824–841.

Johnson, C.W., Beckham, G.T., 2015. Aromatic catabolic pathway selection for optimal production of pyruvate and lactate from lignin. Metab. Eng. 28, 240–247.

Johnson, C.W., Salvachúa, D., Khanna, P., Smith, H., Peterson, D.J., Beckham, G.T., 2016. Enhancing muconic acid production from glucose and lignin-derived aromatic compounds via increased protocatechuate decarboxylase activity. Metabolic Engineering Communications 3, 111–119.

Johnson, C.W., Salvachúa, D., Rorrer, N.A., Black, B.A., Vardon, D.R., St John, P.C., Cleveland, N.S., Dominick, G., Elmore, J.R., Grundl, N., Khanna, P., Martinez, C.R., Michener, W.E., Peterson, D.J., Ramirez, K.J., Singh, P., VanderWall, T.A., Wilson, A. N., Yi, X., et al., 2019. Innovative chemicals and materials from bacterial aromatic catabolic pathways. Joule 3 (6), 1523–1537.

Juhas, M., Reuß, D.R., Zhu, B., Commichau, F.M., 2014. *Bacillus subtilis* and *Escherichia coli* essential genes and minimal cell factories after one decade of genome engineering. Microbiology 160, 2341–2351.

Kohlstedt, M., Starck, S., Barton, N., Stolzenberger, J., Selzer, M., Mehlmann, K., Schneider, R., Pleissner, D., Rinkel, J., Dickschat, J.S., Venus, J., van Duuren, J.B.J. H., Wittmann, C., 2018. From lignin to nylon: cascaded chemical and biochemical conversion using metabolically engineered *Pseudomonas putida*. Metab. Eng. 47, 279–293. March.

Kohlstedt, M., Weimer, A., Weiland, F., Stolzenberger, J., Selzer, M., Sanz, M., Kramps, L., Wittmann, C., 2022. Biobased PET from lignin using an engineered cis, cis-muconate-producing *Pseudomonas putida* strain with superior robustness, energy and redox properties. Metab. Eng. 72, 337–352. May.

Kolisnychenko, V., Plunkett, G., Herring, C.D., Fehér, T., Pósfai, J., Blattner, F.R., Pósfai, G., 2002. Engineering a reduced *Escherichia coli* genome. Genome Res. 12 (4), 640–647.

Kolmogorov, M., Yuan, J., Lin, Y., Pevzner, P.A., 2019. Assembly of long, error-prone reads using repeat graphs. Nat. Biotechnol. 37 (5), 540–546.

Komatsu, M., Uchiyama, T., Omura, S., Cane, D.E., Ikeda, H., 2010. Genome-minimized Streptomyces host for the heterologous expression of secondary metabolism. Proc. Natl. Acad. Sci. U.S.A. 107 (6), 2646–2651.

Kuatsjah, E., Johnson, C.W., Salvachúa, D., Werner, A.Z., Zahn, M., Szostkiewicz, C.J., Singer, C.A., Dominick, G., Okekeogbu, I., Haugen, S.J., Woodworth, S.P., Ramirez, K.J., Giannone, R.J., Hettich, R.L., McGeehan, J.E., Beckham, G.T., 2022. Debottlenecking 4-hydroxybenzoate hydroxylation in *Pseudomonas putida* KT2440 improves muconate productivity from p-coumarate. Metab. Eng. 70, 31–42. January.

Kurokawa, M., Ying, B.W., 2020. Experimental challenges for reduced genomes: the cell model *Escherichia coli*. Microorganisms 8 (1).

Kurokawa, M., Seno, S., Matsuda, H., Ying, B.W., 2016. Correlation between genome reduction and bacterial growth. DNA Res. 23 (6), 517–525.

Lee, J.H., Sung, B.H., Kim, M.S., Blattner, F.R., Yoon, B.H., Kim, J.H., Kim, S.C., 2009. Metabolic engineering of a reduced-genome strain of *Escherichia coli* for L-threonine production. Microb. Cell Factories 8 (1), 1–12.

Liang, P., Zhang, Y., Xu, B., Zhao, Y., Liu, X., Gao, W., Ma, T., Yang, C., Wang, S., Liu, R., 2020. Deletion of genomic islands in the *Pseudomonas putida* KT2440 genome can create an optimal chassis for synthetic biology applications. Microb. Cell Factories 19 (1), 1–12.

Liang, T., Sun, J., Ju, S., Su, S., Yang, L., Wu, J., 2021. Construction of T7-like expression system in *Pseudomonas putida* KT2440 to enhance the heterologous expression level. Front. Chem. 9 (July), 1–8.

Lieder, S., Nikel, P.I., de Lorenzo, V., Takors, R., 2015. Genome reduction boosts heterologous gene expression in *Pseudomonas putida*. Microb. Cell Factories 14 (1), 1–14. https://doi.org/10.1186/s12934-015-0207-7.

Ling, C., Peabody, G.L., Salvachúa, D., Kim, Y.M., Kneucker, C.M., Calvey, C.H., Monninger, M.A., Munoz, N.M., Poirier, B.C., Ramirez, K.J., St John, P.C., Woodworth, S.P., Magnuson, J.K., Burnum-Johnson, K.E., Guss, A.M., Johnson, C. W., Beckham, G.T., 2022. Muconic acid production from glucose and xylose in *Pseudomonas putida* via evolution and metabolic engineering. Nat. Commun. 13 (1).

Linger, J.G., Vardon, D.R., Guarnieri, M.T., Karp, E.M., Hunsinger, G.B., Franden, M.A., Johnson, C.W., Chupka, G., Strathmann, T.J., Pienkos, P.T., Beckham, G.T., 2014. Lignin valorization through integrated biological funneling and chemical catalysis. Proc. Natl. Acad. Sci. U.S.A. 111 (33), 12013–12018.

Luu, R.A., Kootstra, J.D., Nesteryuk, V., Brunton, C.N., Parales, J.V., Ditty, J.L., Parales, R.E., 2015. Integration of chemotaxis, transport and catabolism in *Pseudomonas putida* and identification of the aromatic acid chemoreceptor PcaY. Mol. Microbiol. 96 (1), 134–147.

Martin-Pascual, M., Batianis, C., Bruinsma, L., Asin-Garcia, E., Garcia-Morales, L., Weusthuis, R.A., van Kranenburg, R., Martins dos Santos, V.A.P., 2021. A navigation guide of synthetic biology tools for *Pseudomonas putida*. Biotechnol. Adv. 49, 107732. December 2020.

Martínez-García, E., de Lorenzo, V., 2011. Engineering multiple genomic deletions in Gram-negative bacteria: analysis of the multi-resistant antibiotic profile of *Pseudomonas putida* KT2440. Environ. Microbiol. 13 (10), 2702–2716.

Martínez-García, E., Nikel, P.I., Aparicio, T., de Lorenzo, V., 2014a. Pseudomonas 2.0: genetic upgrading of *P. putida* KT2440 as an enhanced host for heterologous gene expression. Microb. Cell Factories 13 (1), 1–15.

Martínez-García, E., Nikel, P.I., Chavarría, M., de Lorenzo, V., 2014b. The metabolic cost of flagellar motion in *Pseudomonas putida* KT2440. Environ. Microbiol. 16 (1), 291–303.

McNaught, K.J., Kuatsjah, E., Zahn, M., Prates, É.T., Shao, H., Bentley, G.J., Pickford, A. R., Gruber, J.N., Hestmark, K.V., Jacobson, D.A., Poirier, B.C., Ling, C., San Marchi, M., Michener, W.E., Nicora, C.D., Sanders, J.N., Szostkiewicz, C.J., Veličković, D., Zhou, M., et al., 2023. Initiation of fatty acid biosynthesis in *Pseudomonas putida* KT2440. Metab. Eng. 76, 193–203. December 2022.

Mizoguchi, H., Mori, H., Fujio, T., 2007. *Escherichia coli* minimum genome factory. Biotechnol. Appl. Biochem. 46 (3), 157–167.

Nikel, P.I., de Lorenzo, V., 2014. Robustness of *Pseudomonas putida* KT2440 as a host for ethanol biosynthesis. N. Biotech. 31 (6), 562–571.

Nikel, P.I., de Lorenzo, V., 2018. *Pseudomonas putida* as a functional chassis for industrial biocatalysis: from native biochemistry to trans-metabolism. Metab. Eng. 50 (April), 142–155.

Nikel, P.I., Martínez-García, E., de Lorenzo, V., 2014. Biotechnological domestication of pseudomonads using synthetic biology. Nat. Rev. Microbiol. 12 (5), 368–379.

Nikel, P.I., Chavarría, M., Fuhrer, T., Sauer, U., De Lorenzo, V., 2015. *Pseudomonas putida* KT2440 strain metabolizes glucose through a cycle formed by enzymes of the Entner-Doudoroff, embden-meyerhof-parnas, and pentose phosphate pathways. J. Biol. Chem. 290 (43), 25920–25932.

Nikel, P.I., Chavarría, M., Danchin, A., de Lorenzo, V., 2016. From dirt to industrial applications: *Pseudomonas putida* as a Synthetic Biology chassis for hosting harsh biochemical reactions. Curr. Opin. Chem. Biol. 34, 20–29.

Notonier, S., Werner, A.Z., Kuatsjah, E., Dumalo, L., Abraham, P.E., Hatmaker, E.A., Hoyt, C.B., Amore, A., Ramirez, K.J., Woodworth, S.P., Klingeman, D.M., Giannone, R.J., Guss, A.M., Hettich, R.L., Eltis, L.D., Johnson, C.W., Beckham, G.T., 2021. Metabolism of syringyl lignin-derived compounds in *Pseudomonas putida* enables convergent production of 2-pyrone-4,6-dicarboxylic acid. Metab. Eng. 65, 111–122. November 2020.

Park, M.K., Lee, S.H., Yang, K.S., Jung, S.C., Lee, J.H., Kim, S.C., 2014. Enhancing recombinant protein production with an *Escherichia coli* host strain lacking insertion sequences. Appl. Microbiol. Biotechnol. 98 (15), 6701–6713.

Pleitner, Brenna P., Michener, William E., Payne, Courtney E., Beckham, Gregg T., 2019. Determination of Cis,cis- and Cis,trans-Muconic Acid from Biological Conversion: Laboratory Analytical Procedure (LAP). National Renewable Energy Laboratory. Issued on September 4th.

Pósfai, G., Umenhoffer, K., Kolisnychenko, V., Stahl, B., Sharma, S.S., 2013. Emergent Properties of Reduced-Genome *Escherichia coli*, pp. 1044–1047, 2006.

Rorrer, N.A., Nicholson, S., Carpenter, A., Biddy, M.J., Grundl, N.J., Beckham, G.T., 2019. Combining reclaimed PET with bio-based monomers enables plastics upcycling. Joule 3 (4), 1006–1027.

Salvachúa, D., Johnson, C.W., Singer, C.A., Rohrer, H., Peterson, D.J., Black, B.A., Knapp, A., Beckham, G.T., 2018. Bioprocess development for muconic acid production from aromatic compounds and lignin. Green Chem. 20 (21), 5007–5019.

Shanks, B.H., Keeling, P.L., 2017. Bioprivileged molecules: creating value from biomass. Green Chem. 19 (14), 3177–3185.

Sonoki, T., Morooka, M., Sakamoto, K., Otsuka, Y., Nakamura, M., Jellison, J., Goodell, B., 2014. Enhancement of protocatechuate decarboxylase activity for the effective production of muconate from lignin-related aromatic compounds. J. Biotechnol. 192 (Part A), 71–77.

Suárez, R.A., Stülke, J., Van Dijl, J.M., 2019. Less is more: toward a genome-reduced *Bacillus* cell factory for "difficult proteins.". ACS Synth. Biol. 8 (1), 99–108.

Tiwari, R., Sathesh-Prabu, C., Lee, S.K., 2022. Bioproduction of propionic acid using levulinic acid by engineered *Pseudomonas putida*. Front. Bioeng. Biotechnol. 10, 1–10. August.

Turlin, J., Dronsella, B., Maria, A. De, Lindner, S.N., Nikel, P.I., 2022. Integrated rational and evolutionary engineering of genome-reduced *Pseudomonas putida* strains empowers synthetic formate assimilation. bioRxiv 74, 2022. October.

van Duuren, J.B.J.H., de Wild, P.J., Starck, S., Bradtmöller, C., Selzer, M., Mehlmann, K., Schneider, R., Kohlstedt, M., Poblete-Castro, I., Stolzenberger, J., Barton, N., Fritz, M., Scholl, S., Venus, J., Wittmann, C., 2020. Limited life cycle and cost assessment for the bioconversion of lignin-derived aromatics into adipic acid. Biotechnol. Bioeng. 117 (5), 1381–1393.

Vardon, D.R., Franden, M.A., Johnson, C.W., Karp, E.M., Guarnieri, M.T., Linger, J.G., Salm, M.J., Strathmann, T.J., Beckham, G.T., 2015. Adipic acid production from lignin. Energy Environ. Sci. 8 (2), 617–628.

Vardon, D.R., Rorrer, N.A., Salvachúa, D., Settle, A.E., Johnson, C.W., Menart, M.J., Cleveland, N.S., Ciesielski, P.N., Steirer, K.X., Dorgan, J.R., Beckham, G.T., 2016. *cis, cis*-Muconic acid: separation and catalysis to bio-adipic acid for nylon-6,6 polymerization. Green Chem. 18 (11), 3397–3413.

Vaser, R., Šikić, M., 2021. Time- and memory-efficient genome assembly with Raven. Nature Computational Science 1 (5), 332–336.

Weimer, A., Kohlstedt, M., Volke, D.C., Nikel, P.I., Wittmann, C., 2020. Industrial biotechnology of *Pseudomonas putida*: advances and prospects. Appl. Microbiol. Biotechnol. 104 (18), 7745–7766.

Wick, R.R., Holt, K.E., 2019. Benchmarking of long-read assemblers for prokaryote whole genome sequencing. F1000Research 8, 1–23.

Wick, R.R., Holt, K.E., 2022. Polypolish: short-read polishing of long-read bacterial genome assemblies. PLoS Comput. Biol. 18 (1), 1–13.

Wick, R.R., Judd, L.M., Cerdeira, L.T., Hawkey, J., Méric, G., Vezina, B., Wyres, K.L., Holt, K.E., 2021. Trycycler: consensus long-read assemblies for bacterial genomes. Genome Biol. 22 (1), 1–17. https://doi.org/10.1186/s13059-021-02483-z.

Wynands, B., Otto, M., Runge, N., Preckel, S., Polen, T., Blank, L.M., Wierckx, N., 2019. Streamlined *Pseudomonas taiwanensis* VLB120 chassis strains with improved bioprocess features. ACS Synth. Biol. 8 (9), 2036–2050.

Yan, P., Wu, Y., Yang, L., Wang, Z., Chen, T., 2018. Engineering genome-reduced *Bacillus subtilis* for acetoin production from xylose. Biotechnol. Lett. 40 (2), 393–398.

Yu, B.J., Sung, B.H., Koob, M.D., Lee, C.H., Lee, J.H., Lee, W.S., Kim, M.S., Kim, S.C., 2002. Minimization of the *Escherichia coli* genome using a Tn5-targeted Cre/IoxP excision system. Nat. Biotechnol. 20 (10), 1018–1023.

Zhang, F., Huo, K., Song, X., Quan, Y., Wang, S., Zhang, Z., Gao, W., Yang, C., 2020. Engineering of a genome-reduced strain Bacillus amyloliquefaciens for enhancing surfactin production. Microb. Cell Factories 19 (1), 1–13.

Zong, Q.J., Xu, T., Liu, H., Xu, L., Zhang, R.K., Li, B.Z., Liu, Z.H., Yuan, Y.J., 2022. Microbial valorization of lignin to bioplastic by genome-reduced *Pseudomonas putida*. Front. Microbiol. 13. May.